Hindawi
Wireless Communications and Mobile Computing
Volume 2022, Article ID 1926940, 13 pages
https://doi.org/10.1155/2022/1926940

Research Article

Application of Image Color Gamut Boundary Judgment Algorithm in Digital Media

Xuewei Li

College of Art, Northeast Electric Power University, Jilin Jilin 132000, China

Correspondence should be addressed to Xuewei Li; lixuewei@neepu.edu.cn

Received 18 May 2022; Revised 25 July 2022; Accepted 1 August 2022; Published 28 August 2022

Academic Editor: Jun Ye

Image chromatic aberration evaluation is one of the research hotspots and academic difficulties in the field of color science and imaging technology. Based on the algorithm theory of image color gamut boundary judgment, this paper constructs its application model in digital media. The model uses the threshold color difference image as a reference and applies it to the evaluation experiment of color difference above the threshold based on the quantitative estimation method. During the simulation process, the improved HAD dual-color image digital boundary judgment algorithm is programmed. For small color difference data at the threshold level, the calculated color difference of the boundary judgment algorithm framework is smaller than the visual perception color difference; for the large color difference data above the threshold, the boundary judgment algorithm framework is given. The research results of the threshold color difference experiment show that the perceptible color difference threshold and acceptable color difference threshold of image color gamut observers for image color difference are 1.85 AE and 3.63 AE, respectively, which are basically twice the relationship. The visually perceptible chromatic aberration threshold and acceptable chromatic aberration threshold for lightness parameters are higher than those of chroma and hue, which shows that the boundary judgment algorithm framework has certain advantages for the evaluation performance of color digital image threshold chromatic aberration and effectively improves the algorithm robustness.

1. Introduction

With the development of various display media technologies, the application of color digital images in people's work and life is becoming more and more extensive, so the color difference evaluation of color digital images becomes increasingly important [1]. However, since a color digital image is composed of a large number of pixels of different colors, it is an uneven and complex color sample, which is difficult to measure directly with a colorimetric instrument [2], and it is also more complicated than a uniform color sample to calculate, so it has always been a color science and research difficulties in the field of imaging technology [3, 4].

Image chromatic aberration evaluation is one of the research hotspots and academic difficulties in the field of color science and imaging technology. Objectively and effectively measuring and evaluating the color difference between different color samples is also a difficult problem and a key technology to be solved urgently in the industry. These color difference formulas have been widely used in textile, printing, and other industries [5, 6]. With the development of science and technology, display devices such as smart mobile phones, digital TVs, tablet computers, and desktop monitors also require an accurate color difference formula to evaluate the reproduction performance of their color digital images [7]. This brings huge losses to the self-interest of the original creator [8]. Therefore, the issue of intellectual property protection of digital media has attracted more and more attention, and the issue of digital media certification has become increasingly prominent [9–11].

This paper studies the application of the image model boundary judgment algorithm framework in image chromatic aberration evaluation. The research first verified CIELAB, CIEDE2000, S-CIELAB, S-CIEDE2000, and CAM02 through the psychophysical experimental method test of category determination. The performance of the six color difference formulas and models of UCS and boundary judgment algorithm in the evaluation of image color difference

and the parameters affecting the evaluation of image color difference were analyzed through visual data, and the relationship between lightness, chroma, hue, resolution, and sharpness was discussed. These three methods are the most used in current applications, so the algorithms in these three transform domains are introduced. The research results show that the boundary judgment algorithm framework based on the appearance model has the highest prediction accuracy for image color difference, followed by S-CIELAB, and CAM02-UCS has the worst performance in image chromatic aberration evaluation. The experimental results show that, compared with the traditional Krawtchouk transform, the boundary judgment algorithm of fractional Krawtchouk transform domain will have better robustness and invisibility of digital media after the appropriate fractional order is selected; compared with other transform domain (such as DCT and DWT) boundary judgment algorithms, the robustness of the algorithm in this paper is also higher.

2. Related Work

The researchers used the eigenvalue decomposition method to construct a one-dimensional fractional Krawtchouk transform and further extended it to a two-dimensional space; finally, a class of robust boundary judgment algorithms in the transform domain was designed by applying the fractional Krawtchouk transform [12]. By adjusting the fractional order, the robustness and invisibility of digital media can be enhanced. In addition, in the boundary judgment algorithm, the fractional order can be used as a key to enhance the security of digital media [13].

Dong et al. [14] modified the coefficients in the transform domain to embed digital media. These transforms include discrete Fourier transform (DFT), discrete cosine transform (DCT), and discrete boundary judgment transform (DWT). Bogert et al. [15] believe that it needs to transform the original image, the calculation is more complex, and the amount of data is large, but the digital boundary judgment algorithm in the transform domain can resist the influence of compression coding and low-pass filtering; it can effectively resist such as JPEG compression; the energy distribution in the transform domain is concentrated and easily combined with the human visual system (HVS) to determine the strength of embedded digital media. Wang and Cao [16] found that the method of embedding digital media based on transform domain has many advantages over the method of embedding digital media based on spatial domain, so it is very suitable for application in digital digital media technology. Vazquez and Bertalmío [17] proposed a digital boundary judgment algorithm based on the boundary judgment tree of important coefficients, which uses the boundary judgment of zero-tree coding and the masking of the human visual system to judge the boundary of the blue component (the least sensitive of the human eye) of the color image. Zuo et al. [18] verified that the algorithm has good invisibility, but various image color gamut processing has a greater impact on the blue component, digital media may be lost in various image processing, and the robustness is poor [19].

Compared with the spatial boundary judgment algorithm, the subsequently developed transform domain digital boundary judgment algorithm is more popular because it has many advantages [20]. Transform domain boundary judgment algorithm is to embed digital media information by changing transform domain coefficients. At present, there are commonly used boundary judgment algorithms based on DFT, boundary judgment algorithms based on DWT, and boundary judgment algorithms based on DWT. Then, the LSB algorithm in the spatial domain, the DCT-based boundary judgment algorithm in the transform domain, and the DWT-based digital media algorithm are compared in simulation experiments. The results show that the transform domain boundary judgment algorithm is more robust than the spatial domain boundary judgment algorithm as a whole [21], and the robustness of the boundary judgment algorithm based on DWT in the transform domain is stronger, so this paper selects the boundary judgment transformation to process the image and strives to obtain good robustness and invisibility. Scholars proposed a blind detection algorithm based on boundary judgment domain contrast and HVS characteristic adaptation [22]. The scheme embeds digital media into the detail subgraphs LH and HL by analyzing the boundary judgment transformation and performs the embedding intensity factor according to the boundary judgment contrast and HVS characteristics (i.e., brightness sensitivity, texture sensitivity, and contrast sensitivity) [23, 24]. Experimental results show that the scheme has strong invisibility and robustness without attacks [25] but is not robust after noise, median filtering, clipping, and JPEG compression attacks [26, 27].

3. Analysis of Image Color Gamut Boundary Judgment Algorithm

3.1. Image Gamut Scale. Two stimulus color samples are considered to have matching colors to a standard image gamut observer with normal color vision if they have the same tristimulus value. The image color gamut scale is to establish a prediction model that conforms to the characteristics of color visual discrimination, that is, each unique color should have a unique chromaticity parameter, and a coordinate system with each dimension perpendicular to each other can be used to express the chromaticity parameter of the response. And they reflect the main visual characteristics of color, such as lightness, chroma, and hue. The calculated color difference between two stimulus color samples should be proportional to the corresponding difference in visual perception.

$$\iint \frac{fin(t)}{1/x(t)} - \frac{fin(t+\sigma w(t))}{k(t,t-1)}\,dtdw = 0. \tag{1}$$

Usually, the three RGB channels of a color image pixel are represented as the three imaginary parts f, j, and k of the quaternion. That is, the quaternion method can represent a color image as a pure quaternion matrix. In this way, the three channels of the color image can be processed

as a whole. Suppose (m, n) is a color image of size $M \times N$, which can be expressed as a quaternion.

$$\begin{cases} fin(t + \sigma w(t)) = \dfrac{1}{x} - \dfrac{1}{t}, \\ fin(t - \sigma w(t)) = \sqrt{t}. \end{cases} \tag{2}$$

For the blind boundary judgment algorithm that adopts the quantization method, the plaintext digital media (meaningful binary image digital media) is usually selected. This type of method perturbs the selected transform domain coefficients (or coefficient expressions) according to the bit information (0 or 1) of the digital media after the original image is subjected to the overall orthogonal transform or the block orthogonal transform. Then, inverse transform is performed on the whole transform domain coefficients or the block transform domain coefficients in Figure 1 after perturbation to obtain an image added with digital media.

The image color gamut is decomposed into a series of subband signals with different spatial resolutions (different channels), different frequency characteristics, and directional characteristics. These subband image color gamuts have good local characteristics such as time domain and frequency domain, which can be used to represent the local features of the original image color gamut and then realize the localized analysis of the time and frequency of the image color gamut.

The LSB watermarking algorithm in the spatial domain, the DCT-based watermarking algorithm, and the DWT-based watermarking algorithm in the transform domain are compared by simulation experiments, respectively. The experimental results show that the digital watermarking algorithm based on DWT has stronger robustness than the LSB algorithm and the algorithm based on DCT, so this paper chooses to embed the watermark based on wavelet transform. The quantization formula is divided into an embedding formula and an extraction formula. For the convenience of description, we represent the digital media as a vector w, and f represents its i-th element with a value of 0 or 1; the selected transformation coefficients are represented as vectors C and S, representing its i-th element.

3.2. Combination of Boundary Judgment Conditions. In a mixed color composed of several color components, if one color changes continuously, the appearance of the mixed color will also change continuously. From this, the complementary color law and the intermediate color law of the boundary judgment conditions are obtained. The law of complementary colors: if a color is mixed with its complement in appropriate proportions, it will produce white or gray; if it is mixed in other proportions, it will produce a desaturated color that approximates the color with a larger specific gravity. The law of halftones: the mixing of any two noncomplementary colors produces a halftone whose hue depends on the relative amounts of the two colors, and the saturation in Table 1 depends on how far and near the two colors are in the hue order.

In order to verify the advantages and disadvantages of the algorithm and ensure the authenticity of the evaluation results, each image color gamut observer is required to adapt to the image for 30 minutes before determining the judgment result. Theoretically, if the transform used is an orthogonal transform, the coefficients obtained after transforming the protected image with digital media are equal to the perturbed coefficients (i.e., the values at points P1, P2, P3, and P4). When the values of quality are 90, 80, 70, and 60, respectively, the PSNR value of the algorithm HAD is higher than that before the improvement, but the NC value is lower than the original algorithm, but the NC value is also at a high level. This algorithm is attacked by JPEG compression. The robustness of the future image gamut is stronger.

3.3. Algorithm Recursion Analysis. In this experiment, we embed two digital media images into 96 carrier images, respectively, to obtain 192 algorithm recursion test combinations. In each group of experiments, the fractional order $a = b = 0.4$ is selected, and then, the PSNR value of the digital media image is obtained as the embedding step increases. The figure shows the change of the average PSNR value of the 192 test groups with the increase of the embedding step size. It can be seen from the figure that (1) with the increase of the embedding step size, the PSNR value of the digital media image decreases; (2) under the same quantization step size, the proposed FrKT domain boundary judgment algorithm is better than the Krawtchouk transform domain and score it.

$$\text{tinret}(h(x), x) = \begin{cases} 1 - \cos j(x) \sin h(x), \\ 1.5 \sin (x) \cos (h - x). \end{cases} \tag{3}$$

The boundary judgment algorithm of the order boundary judgment transform (DrFT) has a higher PSNR value, because after the FrKT transform coefficients are embedded in the digital media, the information of the digital media is more evenly distributed to the whole image through the inverse transformation. X, Y, and Z are the tristimulus values of the color sample, Xn, Yn, Zn is the tristimulus value of the CIE standard illuminator irradiated on the complete diffuse reflector and reflected to the eyes of the observer in the image color gamut, where $Yn = 100$, when the viewing angle of the image color gamut of the color sample is less than 30.

In this experiment, the CV value is used to represent the observer accuracy of the image gamut in Figure 2. Image gamut interobserver accuracy refers to the agreement between the experimental data of each image gamut observer and the experimental data of other image gamut observers. The CV values of the image gamut observer accuracy are shown. When viewing the field of view, the CIEl931 XYZ standard chromaticity system should be used; when the viewing angle of the image color gamut of the color sample is greater than 40 fields of view, the CIEl964 XYZ standard chromaticity system

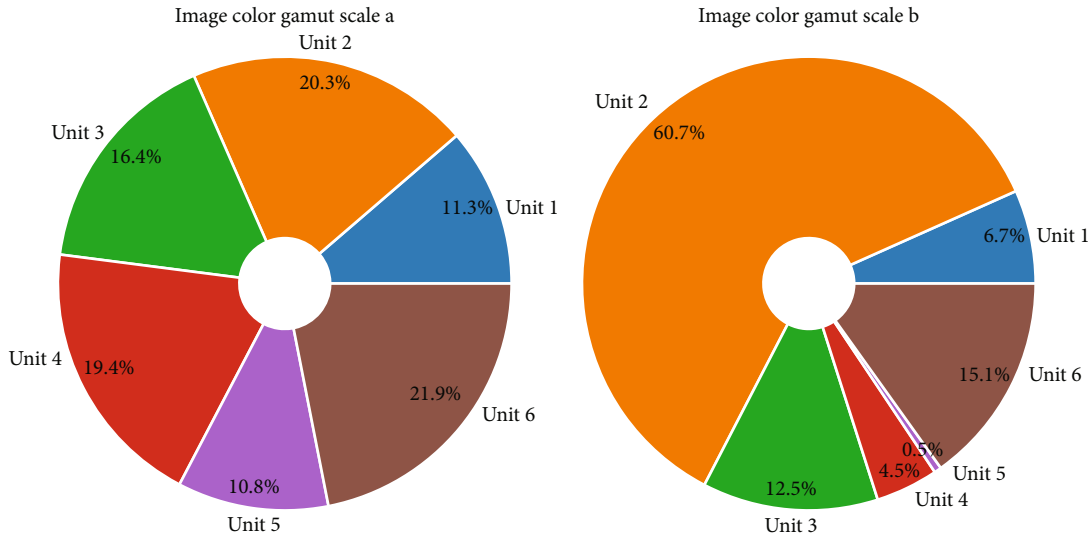

Figure 1: Coefficient distribution of image color gamut scale transform domain.

Table 1: Attributes of boundary judgment conditions.

Attribute number	Evaluation a	Evaluation b	Evaluation c	Evaluation d
10	0.87	1.98	0.46	-1.07
20	0.40	-0.44	0.13	-0.10
30	0.45	1.15	0.19	0.47
40	0.77	-0.43	0.82	-0.45
50	0.43	-1.68	0.49	-1.36
60	0.11	0.19	0.19	-0.05

should be used.

$$\begin{cases} \cos\left(2\text{delta}(x) + x\right) = r + t, \\ \sin\left(2\text{delta}(x) - x\right) = r - t. \end{cases} \tag{4}$$

The subscripts A and B, respectively, represent the two color difference formulas being compared, by comparing the F value with the critical value Fa. Fa is the critical value for determining the F distribution under the confidence interval. Generally, in order to have better robustness of digital media images, a larger quantization step size should be selected; however, a larger quantization step size will lead to a decrease in the visual quality of the image.

The related literatures are the watermarked image and the extracted watermarked image after JPEG compression attack with quality factor = 80 and quality factor = 40, respectively. Generally speaking, the PSNR value of the image embedded in the digital media should be at least close to 40 dB to ensure the invisibility of the digital media. In the following experiments, we selected a quantization step size of 25 for the boundary judgment algorithm of the Krawtchouk transform domain (the average PSNR was 40.72 dB at this time) and selected a quantization step size of 40 and 25 for the boundary judgment algorithm of the FrKT domain (this time the average PSNR was 40.72 dB). The time average PSNR is 42.25 dB and 46.43 dB, respectively.

4. Model Construction of Image Color Gamut Boundary Judgment Algorithm in Digital Media

4.1. Image Color Gamut Normalization Index Analysis. In the test of image color gamut normalization index stage, six modulation parameters including brightness, chroma, hue, contrast, resolution, and sharpness were selected for the test of image color difference parameters and color difference formula. Each parameter is modulated by functions, wherein the modulation of lightness, chroma, and hue is to modulate L, C, and h, respectively, in CIELAB space. Contrast modulation is divided into brightness contrast modulation and chroma contrast modulation, which use the sigmoid function and the inverse-sigmoid function, respectively, to increase and decrease the contrast. The modulation of the resolution adopts the method of double-cubic resampling, and the pixels of 2×2, 3×3, and 4×4 are averaged to the pixels of $l \times l$, respectively.

$$\frac{1 - y(x) - z(x) - x}{y(x) - z(x) - x} = \sum z(x) - x \sum y(x) - x. \tag{5}$$

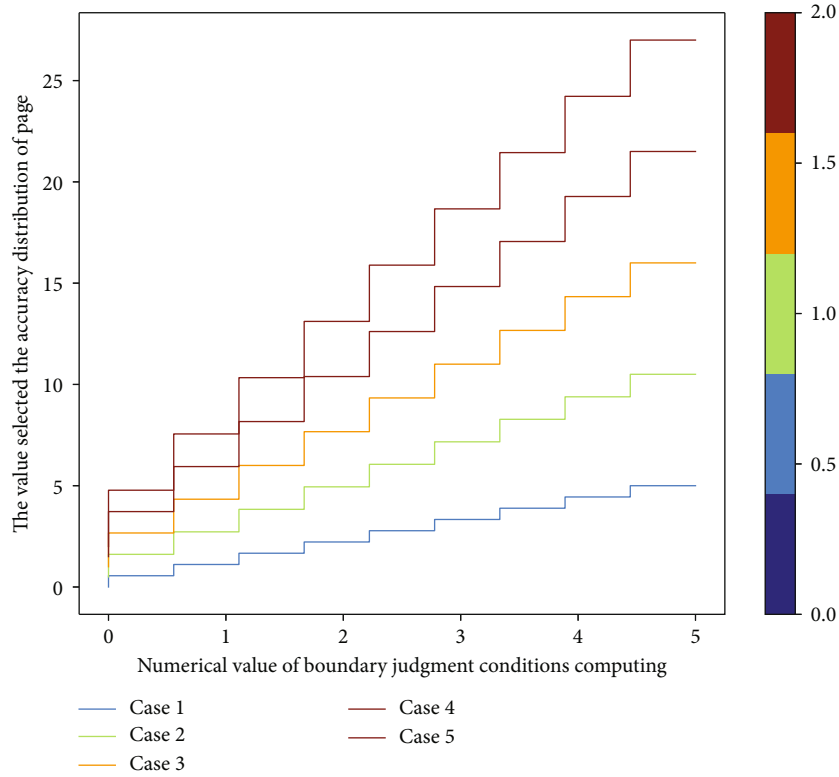

Figure 2: Accuracy distribution of boundary judgment conditions.

They embed "Deer" digital media into each original image and then calculate the PSNR value of the image after digital media, and it shows the change curve of the average PSNR value with the change of fractional order. It can be seen from the figure that (1) when the fractional order $a = b = l$, the PSNR value is the smallest, and FrKT degenerates into the traditional Krawtchouk transform; (2) when the PSNR value is the largest, $a = b = 0.4$ and 0.6. Further, digital media attack is carried out on each image embedded in digital media, and the robustness of the boundary judgment algorithm is analyzed with the change of fractional order.

$$\frac{dy(x)}{dx} - \frac{dz(x)}{dx} = \begin{cases} \frac{1}{2} fin\left(\frac{1-x}{1-y(x)}\right), \\ \frac{1}{2} fin\left(\frac{1-x}{1-z(x)}\right). \end{cases} \quad (6)$$

The article gives the situation that the average BER of all image extraction digital media varies with the fractional order under different attacks. It can be seen from the figure that the average BER is larger when $a = b = 0.1$ and 0.7, which indicates that the robustness of the boundary judgment algorithm is not good at this time. This is because when $a = b = 0.1$ or 0.7, the transformation coefficient we choose is small, even smaller than the quantization step size; after the image with digital media is attacked, the value of Figure 3 changes greatly.

The similarity between the detected digital media and the original digital media is measured by BER, and the BER is close to 0, and the more similar the detected digital media is to the original digital media, the higher the robustness of the digital media. It lists several types of image processing attacks used in the experiment and the corresponding attack parameters. For the rotation and scaling attack, the experiment firstly performs geometric transformation on the image and then performs geometric deformation correction on the transformed image to obtain the attacked image. In order to compare the robustness under different fractional orders, the fractional orders (0.4, 0.5) were selected for the FrKT transform in the experiment.

4.2. Boundary Judgment Coefficient Update. After the experiment of boundary judgment coefficient stage I, it is found that the modulation method of resolution is not very reasonable, and the modulation of chroma and contrast greatly changes the image content, and the sigmoid function of contrast modulation is inverse. The sigmoid function is more complex.

$$0.01 > \frac{\text{ziber}(x,y)}{\text{ziber}(x)} + \text{ziber}(y) - \text{ziber}(y) > 0.001. \quad (7)$$

Therefore, after further reviewing the literature, the modulation parameters and modulation methods selected in the evaluation experiment on the threshold and suprathreshold image chromatic aberration in phase II have been modified to a certain extent. The modulation parameters selected in the stage experiment are lightness,

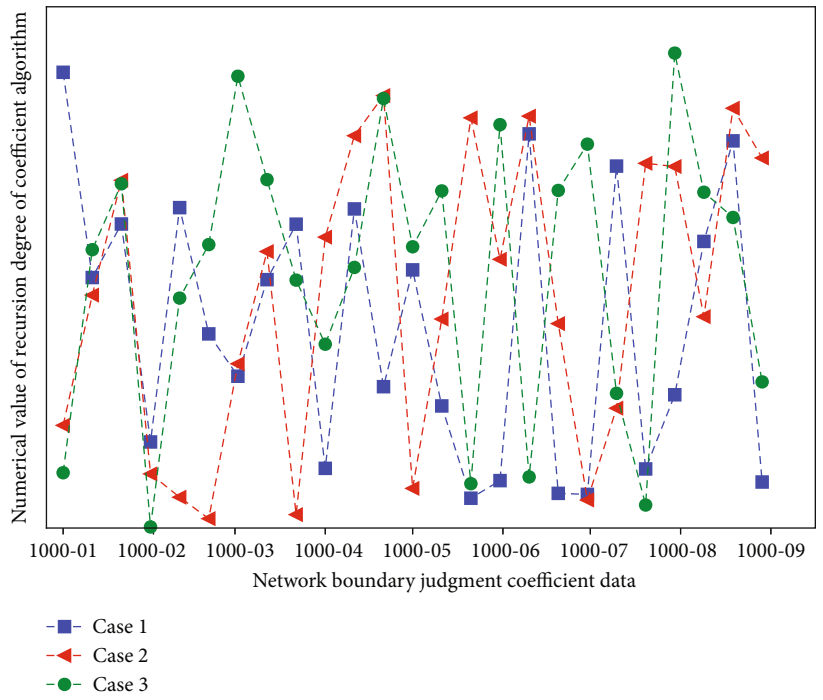

Figure 3: Recursion of boundary judgment coefficient algorithm.

chroma, hue, contrast, and sharpness, and the specific modulation functions and parameters are as shown. The modulation of lightness and chroma is divided into two types: multiplicative and power. For the modulation of contrast, another simple sigmoid function is used to modulate the brightness. The shift modulation of the hue angle and the modulation of the sharpness are the same as those of the phase I method. Finally, there are a total of 540 test images (6 original images × 90 modulations) for phase II experiments.

This kind of color gamut mapping is similar to the device-to-device color gamut mapping, and it is still the calculation from an input point in Figure 4 to an output point in the three-dimensional perceptual color space, regardless of the distance between adjacent pixels in the image color space relation. It can be seen that after the watermark embedding is performed according to the algorithm in this paper, the attacked watermark image has little visual impact, and the similarity between the extracted watermark image and the original watermark image is high, indicating that the algorithm in this paper can attack JPEG compression.

Most of the existing color gamut matching algorithms perform color conversion on an image pixel by pixel and only consider the color characteristics of the image and ignore the color correlation between image pixels. Since the out-of-gamut colors in the image are usually the border colors of the image, it is very important to protect the continuity of the color gamut border of the image. Nonspatially related mapping algorithms sometimes make different colors of the image border map to the same color, resulting in blurred borders or lost borders. Sometimes they are mapped to different colors but distort the facts and make similar colors adjacent in space appear dissimilar. This depends on the spatial properties of neighboring pixels.

$$\left[(\text{delta}(a)\text{\^{}}2 - a) + (\text{delta}(b)\text{\^{}}2 - b) + (\text{delta}(c)\text{\^{}}2 - c) + \frac{1}{abc}\right] = 1 - abc. \tag{8}$$

In contrast, the two boundary judgment algorithms using the DCT domain and the domain are more robust to histogram equalization, which is due to embedding digital media bits into the edge information of the image or using correlations between blocks to embed them. Digital media will increase the robustness of boundary judgment algorithms to histogram equalization.

4.3. Image Color Gamut Interpolation Fitting. In the image gamut interpolation experiments, we combined each binary image with 15 color original images separately to generate zero digital media for the image, generating a total of 105 experimental combinations. Common image processing attacks are then performed on each combined protected image, and digital media is extracted to analyze the robustness of the algorithm.

$$1 - \prod \frac{\text{inret}(\text{ciber}(m,n),m,n)}{m+n} - \prod \frac{\sqrt{\text{inret}(\text{ciber}(m,n),m,n)}}{1-m-n} = \frac{1}{m-n}. \tag{9}$$

More generally, we randomly generate 0-1 matrices of size 64 × 64 as digital media to verify the robustness of the algorithm. Use this matrix to generate the verification information of 15 color images, and then perform various image processing attacks on each image to obtain the average value

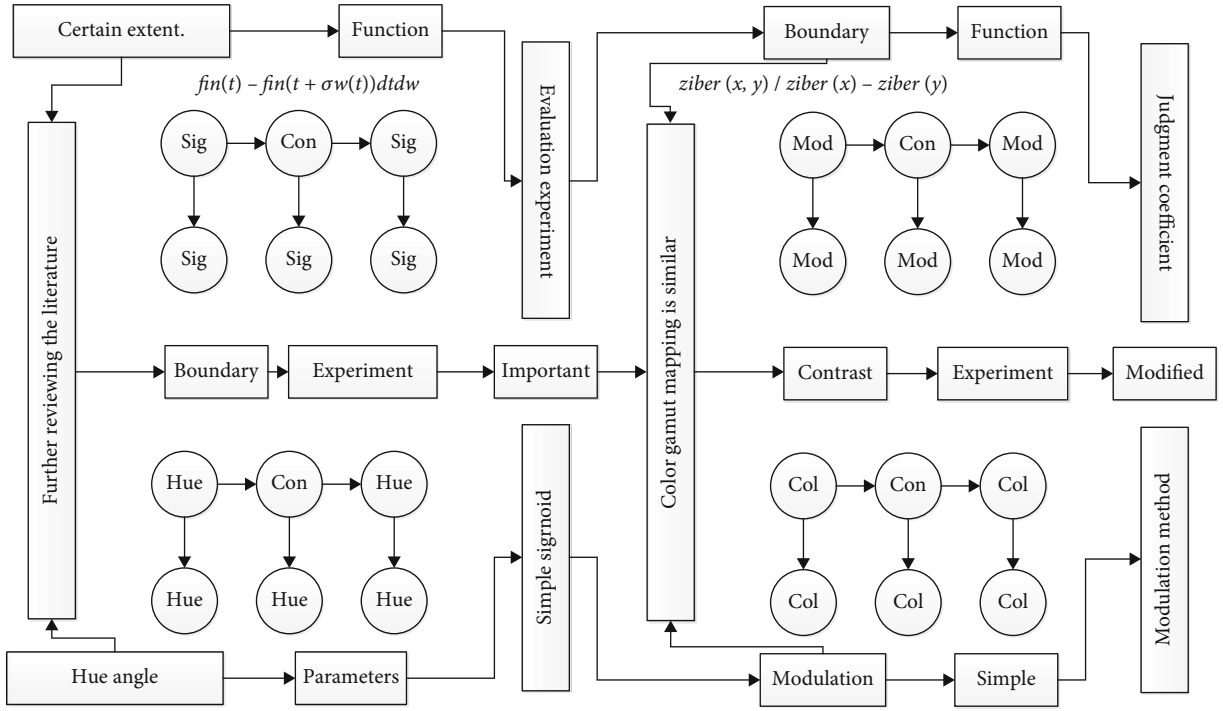

Figure 4: Mapping relationship of boundary judgment coefficients.

of the extracted digital media. It can be seen from the figure that the BER value of the proposed algorithm is lower than that of the existing methods under most attacks, which verifies the robustness of the algorithm in Figure 5.

In this algorithm, the invisibility of digital media depends on the distortion step size parameter, the quantization step size J, and the object parameter in TDFT. Generally speaking, the larger the quantization step size, the better the robustness of the digital media; but the larger quantization step size will lead to the degradation of the image quality of the digital media. According to the experiment, first we choose $g = 700$ and then analyze the influence of a.

$$\frac{\tan \text{gent}(x, y, z)/\text{heter}(x)\text{heter}(y)\text{heter}(z)}{1 - \text{heter}(x, y, z)} \in R. \quad (10)$$

In this experiment, we combined "Deer" digital media with the original images, respectively, to obtain 20 test combinations. The BER value of the paper considers geometric attacks on digital media and the combination of common image gamut processing attacks and ensemble attacks, including the following: image rotation, image scaling, image rotation+scaling, image translation, image cropping, image rotation+scaling+median filter, image rotation+scaling +mean filter, image rotation+scaling+salt and pepper noise, image rotation+scaling+Gaussian white noise, and image rotation+scaling+JPEG compression.

4.4. Quantization of Digital Media. The digital media quantization steps are divided into the following: (1) the original image is resized to make the generated hash robust against scaling operations, and the generated hash is not affected by the image size, and the image is converted to YCrCb

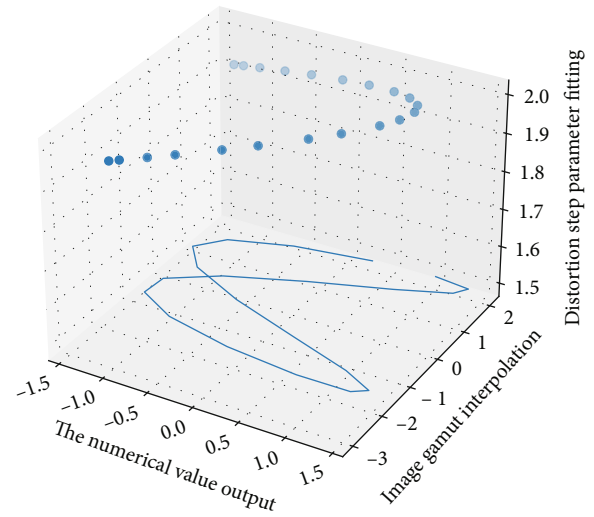

Figure 5: Image color gamut interpolation distortion step parameter fitting.

space; (2) the zemike moment feature of the Y component and the zemike moment feature of extracting the absolute value of the difference between the Cr and Cb components use the values of the first 5-order zemike moments as the global feature, so a total of 22 real eigenvalues except 0-order 1; (3) we perform salient feature extraction on the image, take the first 6 largest salient regions and then extract 4 features of each region including 2 position coordinates and length and width and extract 4 texture features, thus obtaining a total of 48 real local parts.

By extending the boundary judgment transformation in Figure 6 to a two-dimensional situation, the approximate

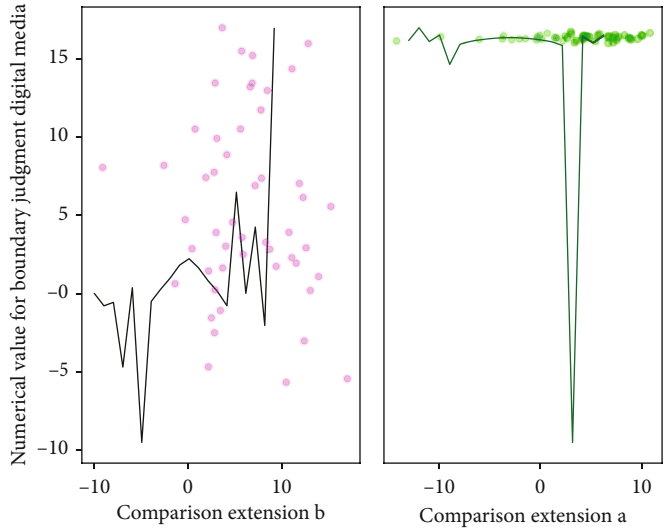

Figure 6: Digital media quantization boundary judgment transformation extension.

components and detail components of the original image in different scales and directions can be obtained. After the image is transformed by multiscale boundary judgment, the coefficients present a pyramid-like structure. And the image energy is redistributed; most of the energy is distributed on the boundary judgment coefficient of the lowest frequency.

$$\left.\begin{aligned} \nabla da &= da(i) - da(j) \\ \nabla db &= db(i) - db(j) \\ \nabla dc &= dc(i) - dc(j) \end{aligned}\right\}. \tag{11}$$

The design of the system content and the construction of the experimental platform are parameterized: the watermark image and the extracted watermark image after the Gaussian noise attack with a mean of 0 and a variance of 0.005 are added. Since both FrBFM and BFM can construct the rotation and scaling invariance of the image, in the case of only geometric attack, FrBFM and BFM have similar robustness, the difference is not very big, and the BER is close to 0.

$$\begin{bmatrix} \sqrt{da(i) + da(j) - 1} \\ \sqrt{db(i) + db(j) - 1} \\ \sqrt{dc(i) + dc(j) - 1}, \cdots, 1) \end{bmatrix} = \sum dxdi. \tag{12}$$

It refers to the relationship between the visual perception chromatic aberration of the observer in the image color gamut and the parameter k after linear modulation of lightness or chroma with parameter k. It can be seen that the error bars of the visual perception chromatic aberration for lightness and chroma vary with the modulation parameter k, that is, the greater the lightness difference or chroma difference, the greater the influence of the image content on the visual perception chromatic aberration of the image gamut observer, it can also be said that the small color difference data between the images is less affected by the image content, while the large color difference data between the images may have a great relationship with the image content.

5. Model Application and Analysis of Image Color Gamut Boundary Judgment Algorithm in Digital Media

5.1. Preprocessing of Image Color Gamut Boundary Data. Using Komca Mmolm company's spectroradiometer CS2000 was measured at a distance of 1.3 m from the display, as shown in the image gamut boundary data. According to the IEC standard, the measurement is carried out in a dark room. The size of the color block to be measured is 5 cm × 5 cm and displayed in the center of the screen. All measurements are performed on this color block, and other areas of the screen are set to black. The tested color blocks are $17 \times 4 = 68$ sets of training samples consisting of red, green, blue, and gray in the range of 0-255 with 16 sampling intervals, and 100 randomly generated test sample data are measured at the same time.

$$\begin{bmatrix} fin(i - \sigma w(i)) \\ fin(j - \sigma w(j)) \\ fin(k - \sigma w(k)) \end{bmatrix} = \begin{bmatrix} i - w'(i) \\ j - w'(j) \\ k - w'(k) \end{bmatrix}. \tag{13}$$

On the whole, the value of the boundary judgment algorithm model for the prediction results of the brightness parameters of the six images is the smallest, that is to say, the correlation between the brightness difference calculated by the boundary judgment algorithm model and the visual perception color difference is the best; especially for the "Street" and "Ski" images, the prediction accuracy of the boundary judgment algorithm was evaluated by F. After

the test, it is significantly better than other color difference formulas.

There are some influences, but it can be recognized, indicating that the algorithm has good resistance to Gaussian noise attack, but it is worse than salt and pepper noise attack. The prediction accuracy of the S-CIELAB model is second only to the boundary judgment algorithm model; especially for the images "Fruits" and "Flower," the prediction accuracy of the S-CIELAB model is very close to the boundary judgment algorithm model, but the S-CIELAB model is for others. The prediction accuracy of the 4 images is slightly different from the boundary judgment algorithm model.

The prediction accuracy of CIELAB and S-CIEDE2000 color difference formula for the image in Figure 7 is very close, while the prediction accuracy of CIEDE2000 is slightly worse than that of CIELAB and S-CIEDE2000, CAM02. The prediction accuracy of UCS on the brightness parameter is most affected by the image content. Its prediction accuracy for the image "Street" is the worst, and its prediction accuracy for the image "Tree" is better, second only to the boundary judgment algorithm model.

$$\frac{\partial \text{delta}(\text{case}(x)-x)}{\partial \text{delta}(x)}+\frac{\partial \text{delta}(\text{case}(y)-y)}{\partial \text{delta}(y)}+\frac{\partial \text{delta}(\text{case}(z)-z)}{\partial \text{delta}(z)}=\sqrt{1-\text{case}(x,y,z)}. \tag{14}$$

This may be because the image "Street" contains a lot of complex high-frequency information and is not suitable for CAM02-UCS, a color difference model based on a single color block calculates color difference, and the image content of "Tree" is relatively simple, so CAM02 is used.

5.2. Implementation of Digital Media Simulation. In order to further compare the performance of the ULPM method and the IULPM method for extracting digital media, we put these two methods in the test image sets data 1 and data 2 for simulation tests. Each test image in the test image set data 1 undergoes a step size of 0.1 from 50 to 100. From this, we can observe the image color gamut that the proposed IULPM method extracts the average NC value of digital media close to 0.9, while the average NC value of the ULPM method is between 0.1 and 0.9. We also tested the 1800 angles of Figure 8 from 0 to 1800 with a step size of 0.10, and the experimental results show similar results.

If the original image is a color image converted to YCrCb space, only the luminance Y component is used, and the resizing makes the generated hash robust against scaling operations and the generated hash is not affected by the image size, for a robust rotation-resistant operation, the image performs a rotation projection to obtain a second image. As shown, this operation converts the rotation of the image into a translation of the second image, and then combines the rotation, and invariant features are obtained by translation invariance.

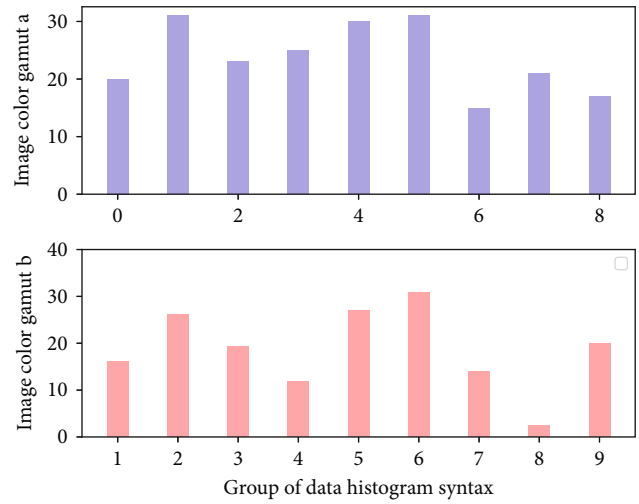

Figure 7: Histogram of image color gamut boundary data.

All methods are tested on the dataset data 1 in Figure 9. For a fair comparison, the PSNR value of all images embedded in digital media is ensured to be close to 40 dB by adaptively adjusting the respective digital media embedding strength, and the results are obtained by all methods use their respective algorithms. The parameter IV indicates the number of intervals of the polar axis, which determines the accuracy of the rotation correction. When IV is set to 360, as is set by the ULPM method, their rotation correction accuracy is only 0.5 degrees. The IULPM method proposed by us increases the IV to 1800 and adds a new "zero-to-one" mapping rule, so that the rotation correction accuracy of the proposed method reaches 0.1. For example, if the data samples of the original image color gamut are 1000, the data of each channel after filtering is 1000, and the total is 2000. Therefore, according to the Nyquist sampling theorem, a downsampling method is proposed, that is, one for every two sample data in each channel is taken.

5.3. Example Application and Analysis. The image color gamut boundary data shows that 216 test images and their original images form 216 test image pairs, and the image color gamut observers evaluate the 216 test image pairs twice to avoid the continuous experiment time being too long and causing the image color gamut. At the beginning of each experiment, all test image pairs are generated in a random display order, and the left and right display positions of the original image and the test image in each test image pair are also random to avoid the nonuniformity of the display affecting the experimental results. The background of the display was set to 20% neutral gray, and the test image pairs were displayed in the center of the display with 10 viewing angle intervals.

In addition, due to the particularity of DFT transformation, the symmetric embedding method should be considered when embedding watermarks to ensure that the data obtained during inverse transformation are real numbers. The image color gamut observation distance of the

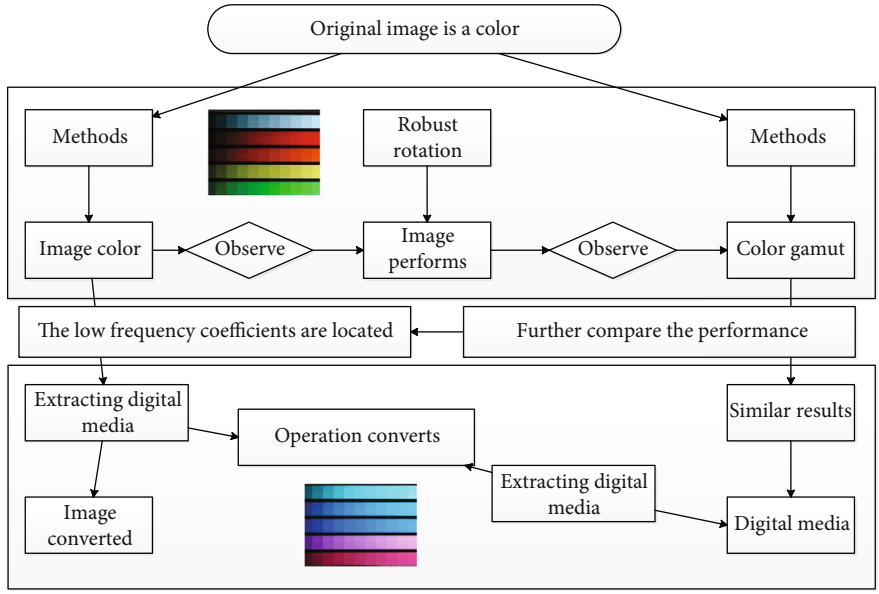

Figure 8: Digital media result topology.

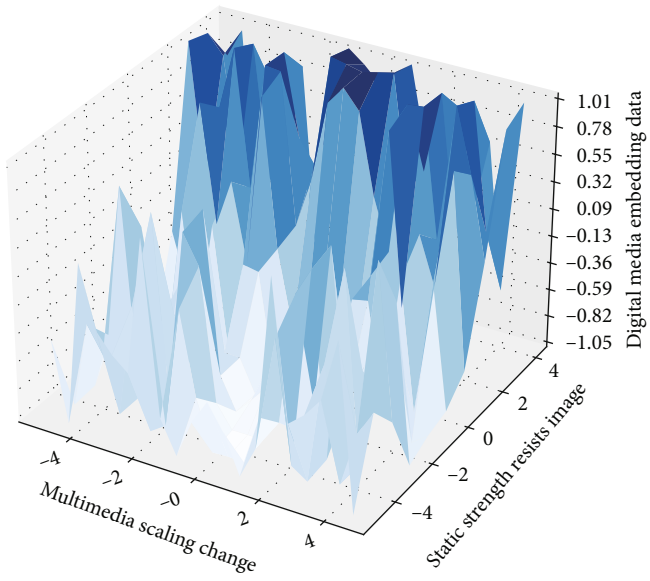

Figure 9: Digital media embedding strength resists image scaling.

image color gamut observer is 80 cm, and then, it is calculated that the horizontal image color gamut observation angle is 22.50, and the vertical image color gamut observation angle is 14.250.

In this experiment, the CV value is used to represent the observer accuracy in Table 2 of the image color gamut. Image gamut interobserver accuracy refers to the agreement between the experimental data of each image gamut observer and the experimental data of other image gamut observers. The intraobserver accuracy of the image color gamut refers to the consistency between the two evaluation data of the image color gamut observer himself for the same test image pair, that is, the repeatability accuracy of the image color gamut observer. The CV values of the image gamut observer accuracy are shown. The larger these two parameters, the higher the robustness of the system, and the worse the imperceptibility of digital media. Based on the experiments in Figure 10, as far as our method is concerned, when the setting range is [0.3, 0.5], and it is set to 24500, the proposed method achieves the best compromise in terms of robustness and imperceptibility of digital media.

In this experiment, a total of 10 image gamut observers with normal color vision participated, all of whom were graduate students, including 6 males and 4

Table 2: Algorithm distribution of image gamut boundary.

Algorithm text	Image gamut boundary code
Their original images form case(x)	For i in range(k):
Causing the image color gamut	Getlabel = labels[sortdisindex[i]]
The image color ∂delta(x)	Classcount[getlabel] = classcount.get(getlabel, 0) +1
Time being too long and $da(i) + da(j)$	Datasize = data.shape[0]
The continuous experiment	X = np.tile(inputx, (datasize, 1)) - data
Gamut boundary $k - \sigma w(k)$	Xpositive = x ∗∗ 2
The image ziber(x) color gamut	Xdistances = xpositive.sum(axis=1)
Test image pairs twice to $1 - x$	Distances = np.sqrt(xdistances)
Observers evaluate the heter(x)/heter(y)	Print(sortclass[0][0])
Test image pairs $\nabla dc = dc(i) - dc(j)$	Knnclassify(inputx, data, labels, k)
Test images and gent(x, y, z)	Return sortclass[0][0]

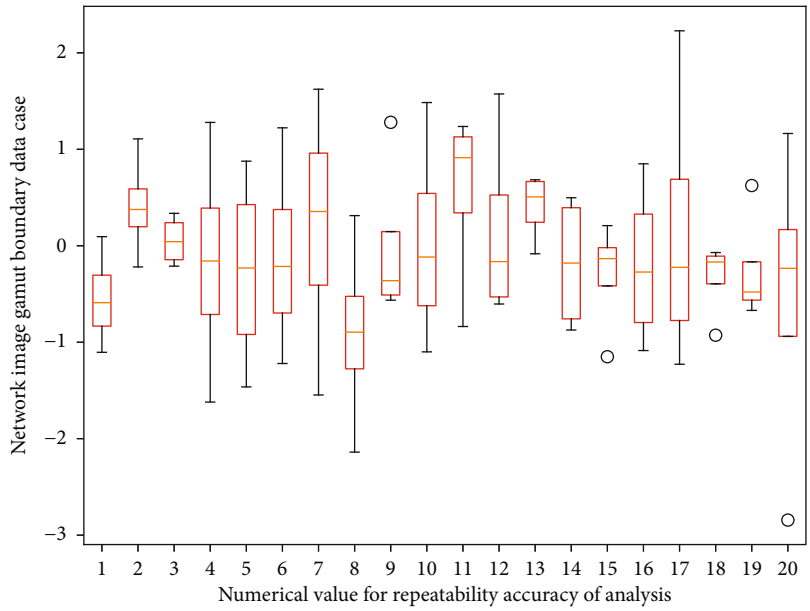

Figure 10: Repeatability accuracy of image color gamut boundary data.

females, aged between 20 and 33. Five of the image gamut observers performed two evaluations to analyze the interobserver accuracy of the image gamut. Therefore, there are 2700 visual evaluation data obtained in this experiment (10 image color gamut observers × 216 test image pairs + 5 image color gamut observers × 108 test image pairs). And the selection of CIECAM02 as the intermediate connection space has wider significance compared to CIELAB. First of all, the Euclidean distance of two colors can be used to describe the color difference in the uniform color space, which is not only simple to calculate but also can reflect the difference between two colors more intuitively, which provides convenience for the application of color industry. Secondly, from the comparison of the design purposes of the two models, CIECAM02 can predict the color perception of the environment according to the parameters of the environment, while CIELAB can only predict the color properties under a specific light source, so choosing CIECAM02 as the intermediate connection space can meet the current color transfer requirements.

6. Conclusion

This paper studies the problem of color difference evaluation of color digital images. Through the design and implementation of related psychophysical experiments, a large amount of visual evaluation data is obtained to test and compare the performance of different color difference formulas in image color difference evaluation and to analyze the influence of color digital images for chromatic aberration evaluation. Compared with the traditional boundary judgment algorithm based on quaternion boundary judgment transformation, the algorithm in this paper has higher robustness and embedding capacity, and there is no energy loss in the boundary judgment algorithm based on quaternion

boundary judgment transformation. The perceptible chromatic aberration thresholds of the image color gamut observers were obtained through psychophysical experiments, and the prediction performance of the image color difference above the threshold of the boundary judgment algorithm framework was discussed. Experiments show that embedding a watermark into the blue component can preserve the perceptual quality of the original image better than embedding digital media into other color components. The scrambling method of changing the gray value does not change the position of the pixel point but changes the gray value of the original image into a new gray value, thereby generating a chaotic image to achieve the purpose of image scrambling. The digital media extracted by the digital media after being attacked has the background information of the original image, which is more conducive to proving the copyright of the image. Therefore, the research in this paper has an important role in promoting the progress of color science and the development of color digital image-related industries.

Data Availability

The data that support the findings of this study are available from the corresponding author upon reasonable request.

Conflicts of Interest

The author declares no conflicts of interest.

References

[1] M. Zhang, Y. Xue, Y. Ge, and J. Zhao, "Watershed segmentation algorithm based on luv color space region merging for extracting slope hazard boundaries," *ISPRS International Journal of Geo-Information*, vol. 9, no. 4, p. 246, 2020.

[2] Y. Zhu, "Color management of digital media art images based on image processing," *Ingénierie des Systèmes d'Information*, vol. 25, no. 4, pp. 445–452, 2020.

[3] K. Zhou, Z. Zhang, R. Yuan, and E. Chen, "A deep learning algorithm for fast motion video sequences based on improved codebook model," *Neural Computing and Applications*, pp. 14–16, 2022.

[4] L. Xu, B. Zhao, and M. R. Luo, "Color gamut mapping between small and large color gamuts: part II gamut extension," *Optics Express*, vol. 26, no. 13, pp. 17335–17349, 2018.

[5] X. Long and J. Sun, "Image segmentation based on the minimum spanning tree with a novel weight," *Optik*, vol. 221, article 165308, 2020.

[6] R. Xu, "Fuzzy C-means clustering image segmentation algorithm based on hidden Markov model," *Mobile Networks and Applications*, vol. 27, no. 3, pp. 946–954, 2022.

[7] Y. Xue, J. Zhao, and M. Zhang, "A watershed-segmentation-based improved algorithm for extracting cultivated land boundaries," *Remote Sensing*, vol. 13, no. 5, p. 939, 2021.

[8] J. Huang, H. Obracht-Prondzynska, D. Kamrowska-Zaluska, Y. Sun, and L. Li, "The image of the City on social media: a comparative study using "Big Data" and "Small Data" methods in the Tri-City Region in Poland," *Landscape and Urban Planning*, vol. 206, article 103977, 2021.

[9] L. Jing and S. Lv, "Art image processing and color objective evaluation based on multicolor space convolutional neural network," *Computational Intelligence and Neuroscience*, vol. 2021, 10 pages, 2021.

[10] W. Chen, C. He, C. Ji, M. Zhang, and S. Chen, "An improved K-means algorithm for underwater image background segmentation," *Multimedia Tools and Applications*, vol. 80, no. 14, pp. 21059–21083, 2021.

[11] F. Zheng, C. Yang, P. H. Chong, G. Wang, G. M. Ali, and P. Lam, "Deep learning algorithm for picture frame detection on social media videos," in *Internet of Things and Intelligence Systems (IoTaIS)*, pp. 149–155, Bandung, Indonesia, November 2021.

[12] P. Kandhway and A. K. Bhandari, "An optimal adaptive thresholding based sub-histogram equalization for brightness preserving image contrast enhancement," *Multidimensional Systems and Signal Processing*, vol. 30, no. 4, pp. 1859–1894, 2019.

[13] R. Li, K. Zou, and W. Wang, "Application of human body gesture recognition algorithm based on deep learning in non-contact human body measurement," *Journal of Ambient Intelligence and Humanized Computing*, pp. 10-11, 2020.

[14] H. Dong, Y. Jiang, Y. Fan, Y. Wang, and G. Gui, "Secondary segmentation extracted algorithm based on image enhancement for intelligent identification systems," *International Journal of Distributed Sensor Networks*, vol. 14, no. 12, 2018.

[15] E. Bogert, A. Schecter, and R. T. Watson, "Humans rely more on algorithms than social influence as a task becomes more difficult," *Scientific Reports*, vol. 11, no. 1, pp. 5–9, 2021.

[16] Y. Wang and Y. Cao, "Leukocyte nucleus segmentation method based on enhancing the saliency of saturation component," *Journal of Algorithms & Computational Technology*, vol. 13, p. 173, 2019.

[17] J. Vazquez and M. Bertalmío, "Spatial gamut mapping among non-inclusive gamuts," *Journal of Visual Communication and Image Representation*, vol. 54, pp. 204–212, 2018.

[18] J. Zuo, Z. Jia, J. Yang, and N. Kasabov, "Moving object detection in video sequence images based on an improved visual background extraction algorithm," *Multimedia Tools and Applications*, vol. 79, no. 39-40, pp. 29663–29684, 2020.

[19] Z. Ying, H. Niu, P. Gupta, D. Mahajan, D. Ghadiyaram, and A. Bovik, "From patches to pictures (PaQ-2-PiQ): mapping the perceptual space of picture quality," *Computer Vision and Pattern Recognition*, pp. 3575–3585, 2020.

[20] D. Liu, Q. Su, Z. Yuan, and X. Zhang, "A fusion-domain color image watermarking based on Haar transform and image correction," *Expert Systems with Applications*, vol. 170, article 114540, 2021.

[21] W. Yang, J. Luo, X. Wu, X. Li, Z. Jiang, and Z. Pan, "Image tactile perception with an improved jseg algorithm," *International Journal of Performability Engineering*, vol. 14, no. 1, p. 77, 2018.

[22] B. Krajancich, N. Padmanaban, and G. Wetzstein, "Factored occlusion: single spatial light modulator occlusion-capable optical see-through augmented reality display," *IEEE Transactions on Visualization and Computer Graphics*, vol. 26, no. 5, pp. 1871–1879, 2020.

[23] S. Faraj, S. Pachidi, and K. Sayegh, "Working and organizing in the age of the learning algorithm," *Information and Organization*, vol. 28, no. 1, pp. 62–70, 2018.

[24] X. Yu, X. Ye, and S. Zhang, "Floating pollutant image target extraction algorithm based on immune extremum region," *Digital Signal Processing*, vol. 123, article 103442, 2022.

[25] D. Komura and S. Ishikawa, "Machine learning approaches for pathologic diagnosis," *Virchows Archiv*, vol. 475, no. 2, pp. 131–138, 2019.

[26] Y. Oishi, H. Ishida, and R. Nakamura, "A new Landsat 8 cloud discrimination algorithm using thresholding tests," *International Journal of Remote Sensing*, vol. 39, no. 23, pp. 9113–9133, 2018.

[27] Y. A. Sari, J. M. Maligan, Y. S. Adinugroho, and Y. G. Bihanda, "Multiple food or non-food detection in single tray box image using fraction of pixel segmentation for developing smart NutritionBox prototype," *International Journal of Innovative Technology and Exploring Engineering (IJITEE)*, vol. 9, no. 3, p. 13, 2020.